DOI: https://doi.org/10.53256/COSE_250101

Recent Advances in Hydraulic Model Testing Techniques

T. Lykke Andersen[a,*], M. R. Eldrup[a] and S. K. Iversen[a]
[a]*Department of the Built Environment, Aalborg University, Denmark*

[*]*Department of the Built Environment, Thomas Manns Vej 23, 9220 Aalborg Ø, Denmark, tla@build.aau.dk*

ABSTRACT: Over the past four decades, numerous hydraulic laboratories capable of generating irregular waves have been established. Most of these facilities employ wave generation and analysis procedures originally developed for linear or mildly nonlinear irregular waves. However, such procedures are often insufficient to accurately reproduce the highly nonlinear wave conditions associated with the design of coastal structures. This paper presents an overview of recent advances in hydraulic model testing techniques that enable the accurate generation and analysis of highly nonlinear irregular waves. The three principal topics addressed are: generation of highly nonlinear waves using piston-type wavemakers combined with cyber-physical modelling; active absorption of reflected waves; and analysis of highly nonlinear long-crested and short-crested waves. These methods have already been applied in several commercial and research projects at Aalborg University. Their practical implementation and performance are demonstrated through selected examples presented in this paper.

KEYWORDS: Nonlinear waves, short-crested waves, wave generation, active absorption, wave analysis, cyber-physical modelling.

1 INTRODUCTION

Coastal structures are frequently designed for wave conditions in which the significant wave height at the structure toe is large relative to the local water depth. In many cases, this ratio approaches the depth-limited condition, implying that waves are strongly nonlinear and may break on the foreshore. The degree of nonlinearity increases further when the wavelength, relative to the water depth at the toe, is also large—for example, for waves with long peak periods. Under such conditions, the highest waves become highly asymmetric, exhibiting narrow, steep crests and broad troughs.

The generation and analysis of these waves in physical models cannot be accurately performed using conventional methods based on linear or mildly nonlinear wave theory. Instead, it is essential to apply nonlinear wave generation and analysis techniques to ensure that the modelled waves faithfully represent prototype conditions. This is crucial to avoid unrealistic structural responses caused by spurious free harmonics arising from the application of inappropriate wavemaker theory.

The present paper reviews recent advances in three key areas that are essential for the accurate modelling of nonlinear waves in physical (and numerical) models:

- Generation of highly nonlinear waves in shallow water using piston-type wavemakers;
- Simultaneous active absorption of reflected waves during nonlinear wave generation;
- Analysis of nonlinear waves, including reflection separation.

The current state of the art, including recent developments in these three areas, is presented below. Subsequently, examples demonstrating the application of the proposed methods are provided.

2 GENERATION OF HIGHLY NONLINEAR IRREGULAR WAVES

Biésel and Suquet (1951) solved the linear wavemaker problem analytically for various wavemaker types. A second-order solution was presented by Sand (1982) for the subharmonics and later extended to include superharmonics by Sand and Mansard (1986). Schäffer (1993) reformulated the theory in a simplified form and incorporated additional terms to account for interactions caused by evanescent modes. This method was subsequently extended to short-crested waves by Schäffer and Steenberg (2003). Eldrup and Lykke Andersen (2019a) proposed a correction to this approach in order to avoid introducing excessive second-order energy when the theory is applied outside the formal validity range of second-order wave theory.

An ad hoc unified generation theory for highly nonlinear irregular waves in shallow water was proposed by Zhang et al. (2007). In this approach, the wavemaker control signals are determined from input generated by a numerical wave model. The coupling to the physical model is based on shallow-water wave generation theory, supplemented by a dispersive correction derived from linear wavemaker theory. The method was later extended by Yang et al. (2014; 2021) to incorporate second-order coupling effects for long-crested and short-crested waves, respectively.

To avoid the generation of spurious free harmonics, it is essential to apply a wavemaker theory that is valid for the water depth at which the wavemaker is installed. If an inappropriate theory is used, spurious harmonics may be generated and can significantly affect the reproduced wave field, as demonstrated by Schäffer (1993) and Eldrup and Lykke Andersen (2019a). A lower-order wavemaker theory may be applied if the bathymetry is constructed to provide sufficient water depth at the wavemaker. However, if only linear or second-order wavemaker theory is available, a substantial portion of the bathymetry may need to be constructed between the wavemaker and the tested structure—particularly for gently sloping foreshores.

In shorter facilities, such as those at Aalborg University, this is often impractical. In larger facilities, it may be feasible but requires significant construction effort. Consequently, many laboratories have implemented transition slopes to reduce the extent of bathymetry construction. However, Eldrup and Lykke Andersen (2024) demonstrated that transition slopes can introduce unwanted free harmonics, thereby producing effects similar to those observed when linear wavemaker theory is used to generate nonlinear waves. In many cases, it is therefore necessary—or at least preferable—to reproduce highly nonlinear waves directly at the wavemaker using appropriate nonlinear generation techniques and the correct bathymetry between the wavemaker and the model.

The validity range of various wavemaker theories was investigated by Eldrup and Lykke Andersen (2019a). Their findings are presented in the classical Le Méhauté (1976) diagram shown in Fig. 1.

The diagram is plotted assuming $H_{max} = 2H_{m0,}$ and the indicated breaking limitation corresponds to breaking of H_{max}. The diagram also includes typical sea states generated at the wavemaker in coastal engineering projects, as listed in Table 1. In this example, the water depth at the wavemaker *(h)* is selected such that the spectral wave height corresponds to 30% of the local depth. This is a commonly applied criterion and ensures that wave breaking does not occur at the wavemaker.

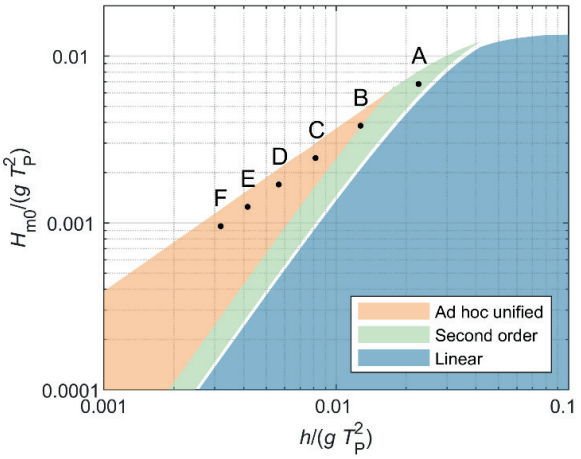

Figure 1. Validity ranges of wavemaker theories according to the limits provided by Eldrup and Lykke Andersen (2019a).

Fig. 1 shows that second-order wavemaker theory is sufficient for sea state A. Sea state B lies only marginally outside the second-order validity range. For the remaining sea states, the ad hoc unified generation method is required. This indicates that, for accurate wave generation in coastal engineering projects, either a sufficiently long foreshore must be included in the physical model to ensure adequate water depth at the wavemaker, or advanced hybrid wave generation techniques must be employed, combining numerical and physical modelling within a cyber-physical framework.

This cyber-physical modelling approach has been extensively applied at Aalborg University over the past decade for long-crested waves. In the present study, it is also applied to short-crested waves. For short-crested wave generation, the numerical model domain must be significantly larger to prevent the physical wavemaker from being located within a diffraction zone of the numerical model. As a result, the computational effort becomes substantial—even when using Boussinesq-type wave models—particularly for long-duration time series.

Table 1. Typical sea states generated in coastal physical models.

	Origin	h [m]	H_{m0} [m]	T_p [s]	$\frac{h}{gT_p^2}$	$\frac{H_{m0}}{gT_p^2}$
A	Wind	18.0	5.40	9.0	0.0227	0.0068
B	Wind	18.0	5.40	12.0	0.0127	0.0038
C	Wind	18.0	5.40	15.0	0.0082	0.0024
D	Wind	18.0	5.40	18.0	0.0057	0.0017
E	Swell	12.5	3.75	17.5	0.0042	0.0012
F	Swell	12.5	3.75	20.0	0.0032	0.0010

3 ACTIVE ABSORPTION

Active absorption consists of applying a correction signal to the wavemaker paddles in order to minimise wave re-reflection at the wavemaker. This is essential when testing structures that produce significant reflections, such as caisson breakwaters or steep rubble-mound breakwaters. Under mildly reflective conditions, the system is primarily used to control long-wave energy, which is difficult to dissipate adequately through passive absorption alone.

Various active absorption systems have been proposed based on measurements of different physical quantities in either the far field or the near field. A comprehensive review of these systems is provided by Schäffer and Klopman (2000).

In the following, only systems based on near-field surface elevation measurements are considered. This type of system is preferred by most hydraulic laboratories because it is relatively simple and can achieve high efficiency over a broad frequency range. In such systems, one or more wave gauges are mounted on each moving paddle, and the measured signals are processed through analogue or digital filters to generate correction signals for the wavemakers.

The pioneering work of Milgram (1965; 1970) demonstrated such a system in a wave flume in which the passive absorber was replaced by an active absorber. Schäffer et al. (1994) presented a similar system to that proposed by Milgram (1965; 1970), but applied it simultaneously with wave generation. The system was subsequently extended by Schäffer and Skourup (1996) to account for wave directionality through the use of a causal two-dimensional infinite impulse response (IIR) filter. Schäffer and Jakobsen (2003) further updated the system to allow active absorption simultaneous with nonlinear wave generation.

Lykke Andersen et al. (2016) proposed a similar system but incorporated into the transfer function the possibility that the wave gauge may be positioned with a gap relative to the moving paddle. They demonstrated that a causal finite impulse response (FIR) filter can be used as an alternative to the IIR filters applied in earlier studies. Furthermore, Lykke Andersen et al. (2018) evaluated the performance of this system for nonlinear waves. The results are presented in Fig. 2 in terms of the re-reflection coefficient of the paddle. The performance curve was established in a wave flume equipped with wavemakers at both ends. The reflection coefficient was determined using the methods described by Lykke Andersen et al. (2017) for regular waves, Lykke Andersen et al. (2019) for bichromatic waves, and Eldrup and Lykke Andersen (2019b) for irregular waves. These methods are described in the following section.

The results demonstrate that, in shallow water, the active absorption system exhibits nearly identical efficiency for bound wave components and free wave components. This applies to superharmonics in regular waves, as well as to both subharmonics and superharmonics in bichromatic waves. A similar behaviour was verified for the second-order superharmonic peak in highly nonlinear irregular waves.

Some deviations from the theoretical curve based on linear wavemaker theory are observed in Fig. 2 in the frequency range 1.0–1.3 Hz. During these tests, cross-mode activity was observed, which influenced both the active absorption performance and the reflection analysis results.

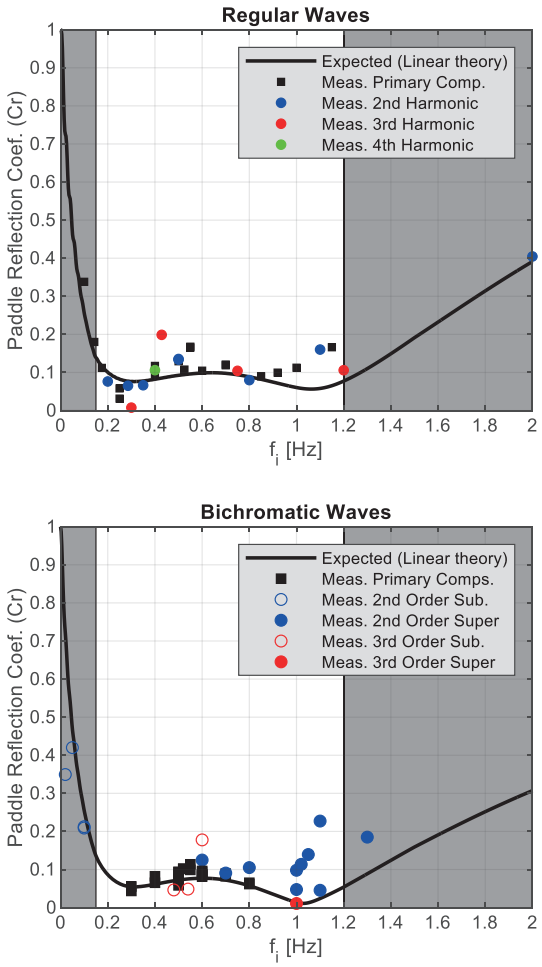

Figure 2. Measured reflection coefficient of the absorbing paddle compared with the theoretical curve based on linear wavemaker theory.

4 SEPARATION OF INCIDENT AND REFLECTED WAVES

A key aspect of physical modelling is the determination of the incident wave field present in the facility. The separation of waves into incident and reflected components requires both a mathematical description of the surface elevation and an appropriate solution procedure. Traditionally, the applied mathematical models have been based on linear wave theory; however, more recently, methods valid for nonlinear waves have been proposed.

Historically, different approaches have been applied to long-crested and short-crested waves, and they are therefore described separately below. Nevertheless, recent developments have introduced methods for short-crested waves that are founded on the same principles as state-of-the-art approaches for long-crested waves.

4.1 *Long-crested waves*

The separation of long-crested waves into incident and reflected components has traditionally been based on measurements of surface elevations at multiple locations. Most established methods rely on linear wave theory and assume a horizontal seabed. Representative approaches include the two-gauge method of Goda and Suzuki (1976), the three-gauge method of Mansard and Funke (1986), and the generalised method for an arbitrary number of gauges proposed by Zelt and Skjelbreia (1992).

However, waves under design conditions for coastal structures are typically highly nonlinear, as illustrated in Fig. 1 for the wavemaker location. At the toe of the structure, the degree of nonlinearity is even greater, and waves may also be breaking. Under such conditions, separation methods based on linear wave assumptions may lead to inaccurate results.

More recently, separation methods based on nonlinear wave assumptions have been proposed, including those by Figueres and Medina (2004) and Eldrup and Lykke Andersen (2019b). The latter demonstrated that their nonlinear method outperforms both traditional linear methods and the approach proposed by Figueres and Medina (2004).

The method by Eldrup and Lykke Andersen (2019b) employs different mathematical representations of the wave field in the subharmonic, primary, and superharmonic frequency regions. In the subharmonic and superharmonic regions, both bound and free wave components are included. These components propagate with different celerities and can therefore be separated using measurements from a multi-gauge array. The only exception occurs in extremely shallow water, where bound and free components have nearly identical celerities, making reliable separation difficult.

Ridder et al. (2023) proposed a minor modification to this method to improve the assessment of when reliable separation of bound and free components is feasible and when the mathematical model should be simplified to include only one of the two components.

Lykke Andersen and Eldrup (2021) extended the mathematical formulation to account for the shoaling of nonlinear regular waves. However, Lykke Andersen and Eldrup (2024) showed that the complex shoaling behaviour of nonlinear irregular waves makes it challenging to extend the method to irregular waves propagating over sloping foreshores. In cases involving steep foreshores, it may therefore be necessary to calibrate the waves without the structure in place.

A similar approach may be required when significant wave breaking occurs.

4.2 *Short-crested waves*

For short-crested waves, the traditional objective has been to determine the directional spectrum from measured cross-spectra obtained using an array of wave gauges. In practice, only a limited number of gauges are typically available, and therefore additional assumptions must be introduced into the mathematical model.

For example, in the BDM method proposed by Hashimoto and Kobune (1988), it is assumed that the directional spreading function is continuous and smooth, and that no phase-locked reflections are present. In contrast, the MLM method by Isobe and Kondo (1984) assumes that the spreading function follows a $\cos^2 s$ distribution and that phase-locked reflections occur from a known reflection line. A common limitation of all cross-spectral methods is that they cannot provide the incident wave time series, which is often of primary interest in physical modelling applications.

An alternative class of methods exploits the fact that most hydraulic laboratories generate waves using the single summation method. Under this approach, only one primary component is present at each frequency. The directions of these individual primary components are defined in the wave generation software such that the overall directional spreading function satisfies the target specification.

The first method to utilise this information in wave analysis was the linear approach proposed by Draycott et al. (2016). However, its applicability is limited by the assumption that the reflected wave direction is directly opposite to the incident direction. To overcome this limitation, Iversen et al. (2024) developed the SORS method, which allows arbitrary reflection directions for each component.

More recently, Iversen et al. (2025a) extended this approach to nonlinear waves, building on the same principles as the method by Eldrup and Lykke Andersen (2019b). A significant advantage of the resulting NL-SORS method is that it enables reconstruction of both incident and reflected time series for nonlinear short-crested waves.

The method assumes that the primary incident directional spectrum is narrow-banded in both frequency and direction, which permits accurate estimation of bound harmonics. Iversen et al. (2025a) quantified the errors associated with cases that do not fully satisfy this assumption. They found that errors in the superharmonic region are generally small, whereas errors in the subharmonic region may be more significant.

5 APPLICATION OF METHODS FOR SHORT-CRESTED WAVES ON A MILDLY SLOPING FORESHORE

The generation of highly nonlinear waves with simultaneous active absorption is demonstrated using the cases listed in Table 1 for which ad hoc unified generation is required, cf. Fig. 1. Cases C and D were reproduced at a Froude scale of 1:36, whereas cases E and F were reproduced at a Froude scale of 1:25. In the numerical model, a 1:80 foreshore slope was applied for all cases. The mean wave direction (θ_0) was perpendicular to the wavemaker in all tests. A directional spreading function of the form $\cos^{2s}(\theta)$ was adopted with s = 50 for all cases. In addition, for sea states C and D, simulations were also performed with s = 15. The frequency spectrum was defined by a JONSWAP spectrum with a peak enhancement factor γ = 3.3. Table 2 summarises the test conditions in model scale. The input wave height in the numerical model was iteratively adjusted until the target wave height reported in Table 2 was achieved at the interface between the numerical and physical models. A similar iterative adjustment was not performed for the directional spreading parameter. Consequently, the s-values reported in the table correspond to those defined at the generation line in the numerical model. Due to wave refraction within the numerical domain, the spreading at the interface between the numerical and physical models is reduced (i.e. higher effective s-values).

Each test series had a repeat period of 327.68 s, corresponding to 2^{14} data points at a sampling frequency of 50 Hz. The total test duration was set to 390 s to allow for a 10 s ramp-up period, a 10 s ramp-down period, and sufficient time for the establishment of a steady wave field.

Table 2. Test cases with short-crested waves (model scale).

	h [m]	H_{m0} [m]	T_p [s]	θ_0 [°]	s [-]
C1	0.50	0.15	2.5	0	15
D1	0.50	0.15	3.0	0	15
C2	0.50	0.15	2.5	0	50
D2	0.50	0.15	3.0	0	50
E2	0.50	0.15	3.5	0	50
F2	0.50	0.15	4.0	0	50

5.1 *Numerical Model*

The numerical model applied in the cyber-physical modelling framework was the Celeris model developed by Tavakkol and Lynett (2017), modified to incorporate a wave-generating boundary condition with time-series input prescribed at each boundary grid point. This modification enabled second-order wave generation to be applied, thereby significantly reducing the required computational domain compared to linear wave generation. In addition, the sponge-layer formulation was refined to improve absorption efficiency. The numerical model layout is illustrated in Fig. 3.

The spatial discretisation of the numerical model consisted of 50 grid cells per L_{min} in the x-direction (perpendicular to the wave-generating boundary) and 35 grid cells per L_{min} in the y-direction, where L_{min} denotes the linear wavelength in the shallowest part of the model corresponding to the highest primary frequency generated. The temporal discretisation was determined based on a Courant–Friedrichs–Lewy (CFL) number of 0.1.

The sponge layer comprised 900 grid cells at the rear boundary and 700 grid cells along the side boundaries. The length of the 1:80 foreshore slope was selected such that the water depth at the wave-generating boundary satisfied the validity criteria for second-order wavemaker theory, as defined by Eldrup and Lykke Andersen (2019a). Consequently, the slope length was shortest for cases C1 and C2 and longest for case F2. The 1:80 slope terminates at the mean position of the physical wavemaker and is followed by a horizontal plateau, consistent with the configuration in the physical model.

The domain width was selected to minimise diffraction effects. Specifically, the lateral distance from the physical model side wall to the numerical model sponge layer was set to either 3.5 or 5.0 times the distance between the numerical and physical generation boundaries (denoted x_1 in Fig. 3). The larger factor was applied for cases C1 and D1, while the smaller factor was used for the remaining cases. As a result, the numerical domain width exceeded its length in all simulations.

The primary spectral components were generated using the single-summation method, which enables application of the NL-SORS method described by Iversen et al. (2025a). The direction of each primary component was selected randomly in accordance with the prescribed directional spreading function.

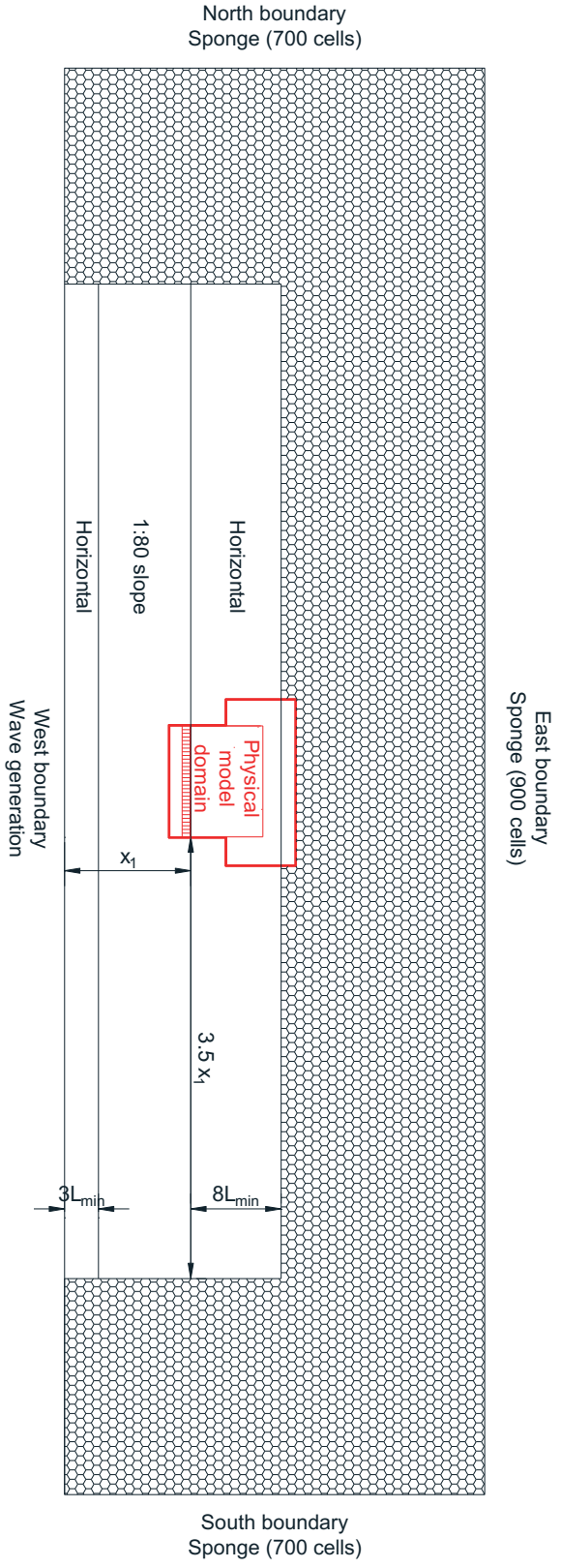

Figure 3. Numerical model layout and location of the physical wave basin and wavemaker (shown in red). The layout is shown to scale for Test C2.

5.2 *Physical Model*

The coupling between the numerical model and the physical model boundary was implemented using the linear coupling approach proposed by Zhang et al. (2007). The improved coupling method suggested by Yang et al. (2021) was not applied in the present study.

Corner reflection was not incorporated in the setup. Consequently, diffraction and reflection zones are expected to develop near the sidewalls (cf. Dalrymple, 1989). To minimise their influence on the analysis, the wave gauge array was positioned close to the wavemaker, yet outside the region affected by significant near-field disturbances. Specifically, the first gauge was located at a distance of three water depths from the mean position of the wavemaker. The array consisted of 11 gauges arranged in accordance with the configuration recommended by Iversen et al. (2025a). In addition, 26 supplementary gauges were installed to provide a more detailed characterisation of the wave field.

The bathymetry in the physical model was horizontal. Although this does not represent a typical coastal configuration, it was selected to avoid the need for constructing a sloping bathymetry for validation purposes and to satisfy the constant-depth assumption required by the method of Iversen et al. (2025a). Given the mild slope applied in the numerical model, the horizontal bathymetry in the physical model is not expected to result in significant release of spurious free harmonics.

The experiments were conducted in the Ocean and Coastal Engineering Basin at Aalborg University. The wavemaker is 13 m long and consists of 30 vertically hinged paddle segments. The basin is equipped with efficient passive absorption along the rear wall and portions of the sidewalls. Figures 4 and 5 present the physical model layout and the configuration of the wave gauge positions.

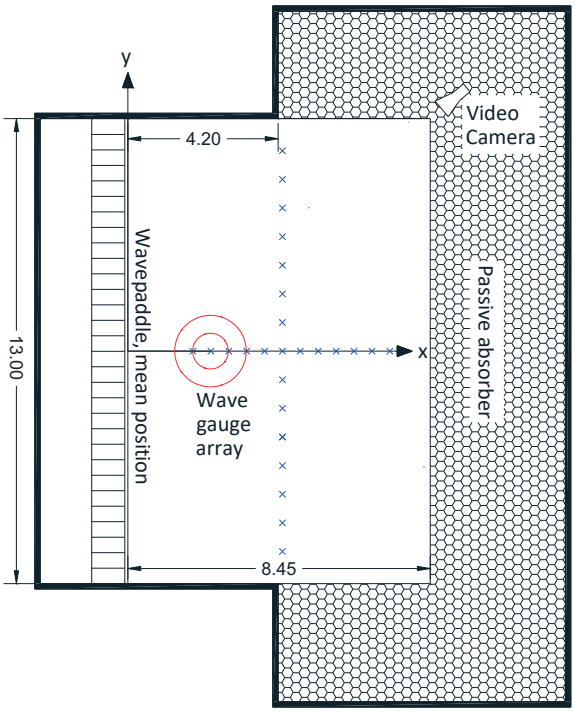

Figure 4. Physical model layout. The NL-SORS array is shown in red (see details in Fig. 5), and the additional 26 gauges are shown in blue, spaced at 0.5 m in the x-direction and 0.8 m in the y-direction.

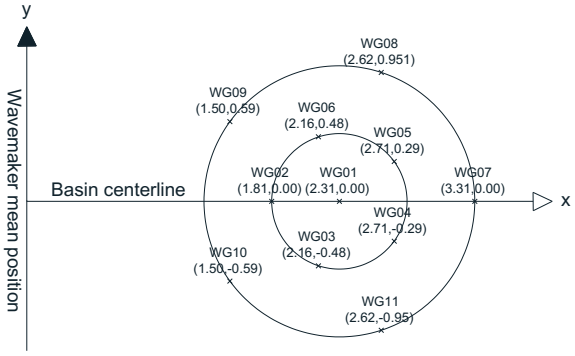

Figure 5. Configuration of the applied wave gauge array. Inner diameter: 1 m; outer diameter: 2m.

5.3 *Results*

Fig. 6 presents a qualitative comparison of the wave field within the basin domain in both the numerical and physical models for sea state F2, which represents the most nonlinear condition (cf. Table 2). The snapshot corresponds to the occurrence of one of the highest waves at the centre of the basin, characterised by a narrow, high crest and a wide trough. Due to the long wave periods, significant refraction occurs in the numerical model, resulting in reduced directional spreading as the waves propagate into the physical domain. In the physical model, minor disturbances caused by the passive rear-wall absorber are visible ahead of the wave.

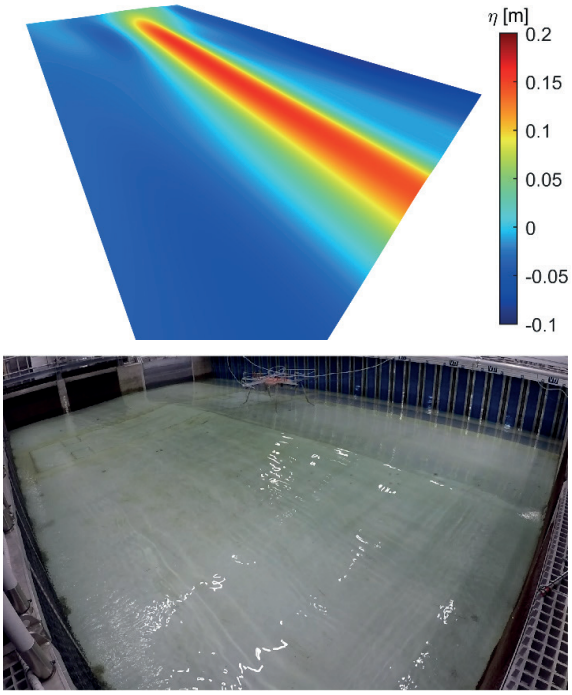

Figure 6. Qualitative comparison of the wave field at the instant corresponding to one of the highest waves in sea state F2 at the centre of the basin. Numerical results are shown for the same area as the physical domain. Camera location as indicated in Fig. 4.

Figure 7 shows the corresponding simulated and measured surface elevations at the same instant for the additional 26 gauges.
The results indicate that the numerical wave field has been reproduced with high fidelity in the physical model for this case.

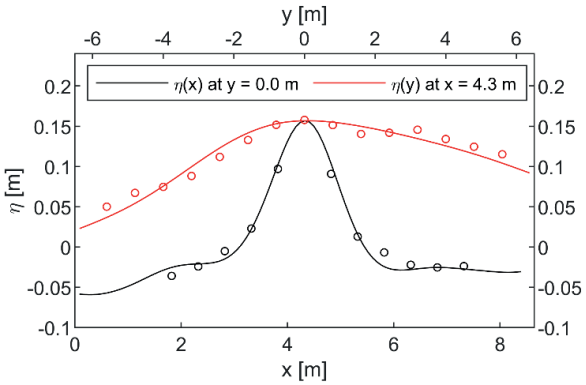

Figure 7. Quantitative comparison corresponding to the instance shown in Fig. 6. Solid lines denote numerical results; circles denote physical measurements.

Figures 8 and 9 present a similar comparison for sea state C1 during one of the largest waves. Sea state C1 has the shortest wave period and the largest directional spreading, making the short-crested characteristics more apparent. Owing to the large directional spreading and the absence of corner reflection, discrepancies increase with distance from the wavemaker, particularly near the sidewalls. Nevertheless, both qualitative and quantitative comparisons demonstrate satisfactory agreement, considering the substantial directional spreading applied in this case.

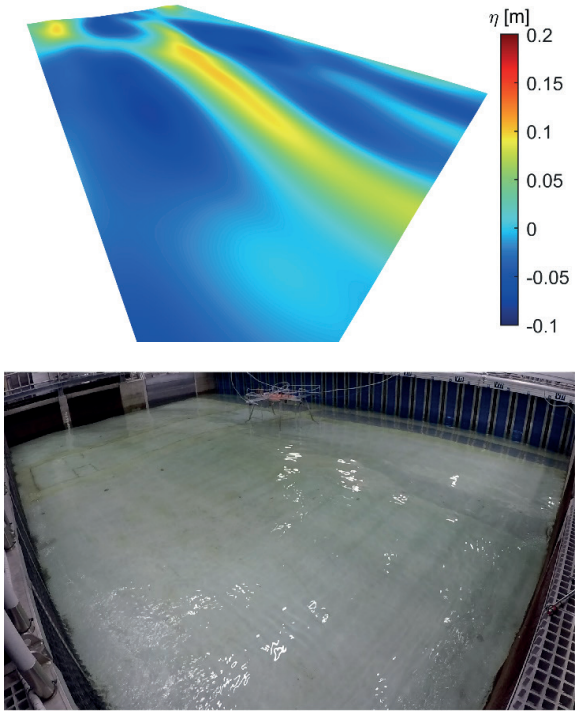

Figure 8. Similar to Fig. 6, but for case C1.

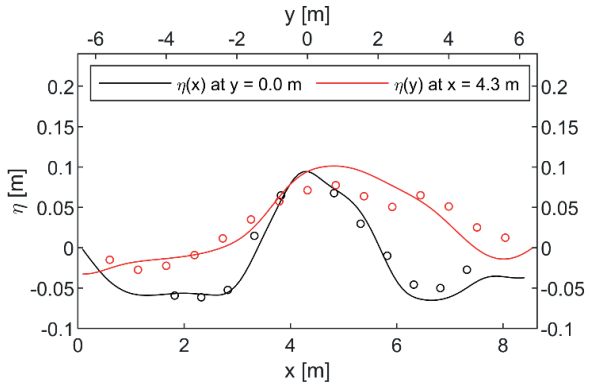

Figure 9. Quantitative comparison corresponding to the instance shown in Fig. 8.

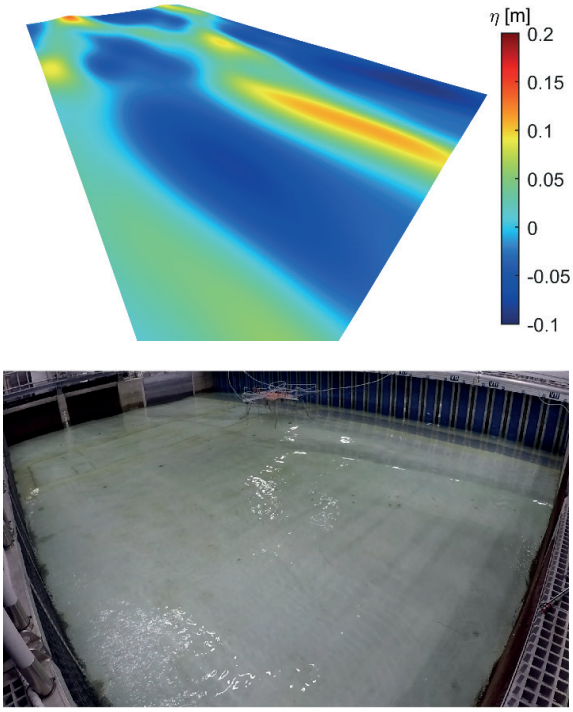

Figure 10. Similar to Fig. 10, but at a random instant with a more directionally spread wave field.

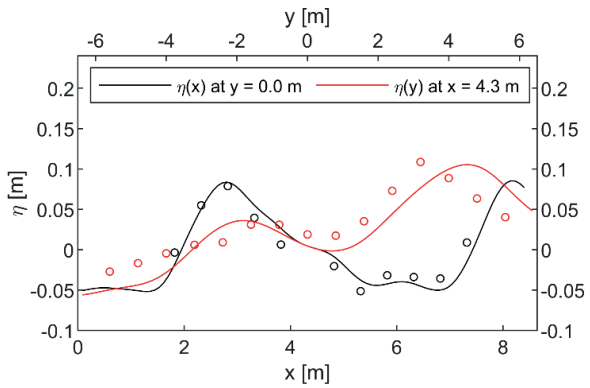

Figure 11. Quantitative comparison corresponding to the instance shown in Fig. 10.

Figures 10 and 11 show the same test case (C1), but at a randomly selected instant characterised by a more pronounced directional spreading of the wave field.

Again, good agreement is observed, particularly near the wavemaker and at the centre of the basin. The accuracy of the coupling between the numerical and physical models was further evaluated through comparison of time series measured at the centre of the circular gauge array, located 2.3 m from the midpoint of the wavemaker. This position is minimally affected by diffraction and reflection from the sidewalls. Figures 12 and 13 present the comparison at the instant of the highest wave in each tested sea state, representing cases with large and small directional spreading, respectively. The time series shown include: (i) the numerically modelled target signal, (ii) the total measured signal in the physical model, and (iii) the incident signal in the physical model obtained using the method of Iversen et al. (2025a). Additional details of this analysis are provided in Iversen et al. (2025b).

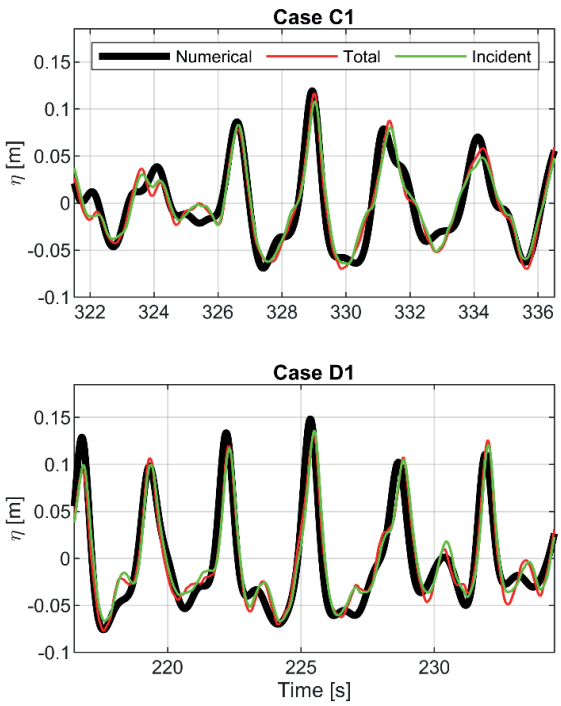

Figure 12. Comparison of time series from the numerical model (black) and physical model (red and green) at the central gauge of the array (WG01) for cases with large directional spreading.

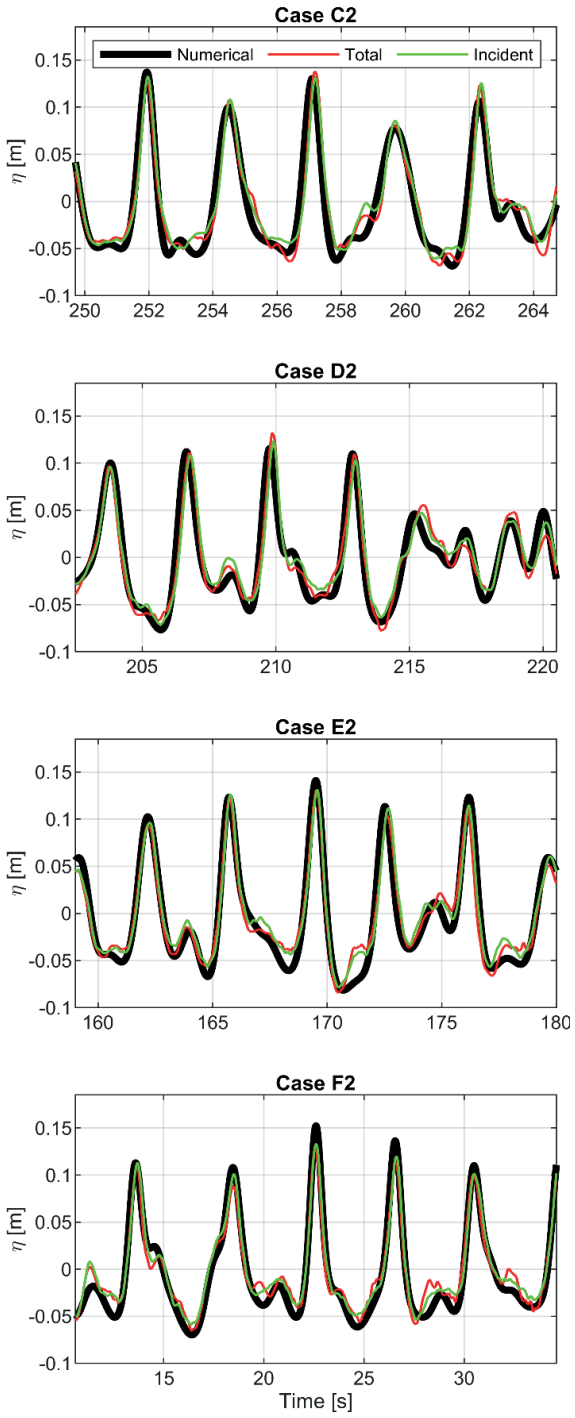

Figure 13. Same as Fig. 12, but for cases with small spreading.

The results demonstrate that it has been possible to shoal the waves in the numerical model into highly nonlinear short-crested conditions and to reproduce them in the physical model using the ad hoc unified generation method. The generated waves exhibit the expected nonlinear characteristics, namely narrow and elevated crests combined with wider and shallower troughs. When compared with the numerical target signals, only minor discrepancies are observed. Such differences are expected due to factors such as leakage beneath and between wavemaker paddles and residual reflections. As a consequence of this leakage, the generated wave heights are approximately 10% lower than the target values, which also leads to the generation of small-amplitude free-wave components. In practice, such leakage effects are typically compensated for during wave generation; however, in the present study, the theoretical transfer function was applied without additional correction. Reflected components were removed from the total measured signal using the method of Iversen et al. (2025a). A detailed analysis of the incident wave components for the present tests is reported in Iversen et al. (2025b).

6 CONCLUSIONS

This paper presents three recent developments aimed at ensuring accurate generation and analysis of highly nonlinear waves in the wave basin at Aalborg University. The results demonstrate that these methods are applicable to a wide range of coastal engineering projects. Together, they enable faithful reproduction of prototype nonlinear wave conditions and allow detailed and reliable analysis of the generated wave field.

Waves generation is achieved through a hybrid (cyber-physical) modelling approach that combines numerical and physical modelling. In the present study, a Boussinesq-type numerical model was employed; however, the developed interface to the AwaSys software enables the use of alternative numerical models where appropriate. Wave analysis is performed using the innovative NL-SORS method, which permits separation of bound and free components in nonlinear short-crested waves generated by the single-summation method. This represents a significant advancement in the analysis of complex wave fields in physical model facilities.

The application of the proposed methods was demonstrated through test cases involving nonlinear waves propagating over a simplified foreshore. The results confirm the accuracy of the coupling between the numerical and physical models, as well as the reliability of the analysis procedure. The NL-SORS analysis method and the nonlinear short-crested wave generation procedure are expected to be implemented in the WaveLab and AwaSys software packages developed at Aalborg University.

ACKNOWLEDGEMENTS

This research did not receive any specific grant from funding agencies in the public, commercial, or not-for-profit sectors.

REFERENCES

Biésel, F. and Suquet, F. (1951). Les Appareils generateurs de Houle en Laboratoire. *La Houille Blanche, Vol. 6, nos. 2,4 et 5.*

Dalrymple, R.A. (1989). Directional wavemaker theory with sidewall reflection. *Journal of Hydraulic Research, Vol. 27, No.1*, pp. 23-34.

Draycott, S., Davey, T., Ingram, D.M., Day, A., Johanning, L., 2016. The spair method: Isolating incident and reflected directional wave spectra in multidirectional wave basins. *Coastal Engineering, Vol. 114*, pp. 265-283.

Eldrup, M.R. and Lykke Andersen, T. (2019a). Applicability of Nonlinear Wavemaker Theory. *Journal of Marine Science and Engineering, Vol. 7, Special Issue "Selected Papers from Coastlab18 Conference"*

Eldrup, M. R. and Lykke Andersen, T. (2019b). Estimation of Incident and Reflected Wave Trains in Highly Nonlinear Two-Dimensional Irregular Waves. *Journal of Waterway, Port, Coastal, and Ocean Engineering, Vol. 145, Issue 1 (January 2019).*

Eldrup, M. R. and Lykke Andersen, T. (2024). Generation of Highly Nonlinear Waves in a Short Wave Flume. *CoastLab24, Delft, The Netherlands*.

Figueres, M. and Medina, J. R. (2004). Estimating incident and reflected waves using a fully nonlinear wave model. *In Vol. 4 of Coastal Engineering 2004, edited by J. M. Smith, 594–603. Singapore: World Scientific*.

Goda, Y. and Suzuki, Y. (1976). Estimation of incident and reflected waves in random wave experiments. *Proceedings of the 15th Coastal Engineering Conference*, 828‑845.

Hashimoto, N. and Kobune, K. (1988). Directional spectrum estimation from a bayesian approach. *Coastal Engineering Proceedings 1(21),4*, pp. 62–76.

Isobe, M. and Kondo, K. (1984). Method for estimating directional wave spectrum in incident and reflected wave field. *Coastal Engineering* , pp. 467–483.

Iversen, S. K., Lykke Andersen, T. and Frigaard, P. (2024). Directional Spectrum Estimation for Sea States Generated by the Single Summation Method. *Journal of Coastal and Hydraulic Structures, Vol. 4, 15.*

Iversen, S. K., Eldrup, M.R., Lykke Andersen, T. and Frigaard, P. (2025a). The NL-SORS Method for Separation of Nonlinear Multidirectional Waves into Incident and Reflected Wave Trains. *Coastal Engineering, Elsevier.*

Iversen, S. K., Lykke Andersen, T., Alfaro Corrales, F. and Eldrup, M.R. (2025b). Directional Decomposition of Experimental Data with Nonlinear Short-Crested Waves Using the NL-SORS Method. *Coastal and Offshore Science and Engineering - SCACR 2025 special issue.*

Le Méhauté (1976). *An Introduction to Hydrodynamics and Water Waves*. Springer Science & Business Media.

Lykke Andersen, T., Clavero, M., Frigaard, P., Losada, M., Puyol, J. I. (2016). A new active absorption system and its performance to linear and non-linear waves. *Coastal Engineering, Vol.114, August 2016,* Pages 47–60.

Lykke Andersen, T., Eldrup, M. R., Frigaard, P. (2017). Estimation of incident and reflected components in highly nonlinear regular waves. *Coastal Engineering, Vol. 117,* pp. 51-64.

Lykke Andersen, T., Clavero, M., Eldrup, M. R., Frigaard, P., Losada, M. (2018). Active Absorption of Nonlinear Irregular Waves. *Proceedings of the 36th International Conference on Coastal Engineering (ICCE), Baltimore, USA.*

Lykke Andersen, T., Eldrup, M.R., Clavero, M. (2019). Separation of Long-Crested Nonlinear Bichromatic Waves into Incident and Reflected Components. *Journal of Marine Science and Engineering, Vol. 7, Special Issue "Selected Papers from Coastlab18 Conference"*

Lykke Andersen, T. and Eldrup, M. R. (2021). Estimation of incident and reflected components in nonlinear regular waves over sloping foreshores. *Coastal Engineering, Vol. 169.*

Lykke Andersen, T. and Eldrup, M. R. (2024). Applicability of Reflection Separation Algorithms to Nonlinear Irregular Waves over Sloping Foreshores. *CoastLab24, Delft, The Netherlands.*

Mansard, E.P.D. and Funke, E.R. (1980). The measurement of incident and reflected spectra using a least squares method. *Proceedings of the 17th Coastal Engineering Conference*: 154-172.

Milgram, J. H. (1965). Compliant Water Wave Absorbers. *M.I.T. Department of Naval Architecture and Marine Engineering Report no. 65–13*.

Milgram, J. H. (1970). Active water-wave absorbers. *Journal of Fluid Mechanics, Vol. 43, Issue 4,* pp. 845-859.

Ridder, M.P.D,, Kramer, J., Bieman, J.P.D. and Wenneker, I. (2023). Validation and practical application of nonlinear wave decomposition methods for irregular waves. *Coastal Engineering, Vol. 183*.

Sand. S. E. (1982). Long wave problems in Laboratory Models. *Journal of the Waterway, Port, Coastal and Ocean Division, Vol. 108, Issue 4,* pp. 492-503.

Sand, S. E. and Mansard, E.P.D. (1986). Reproduction of Higher Harmonics in Irregular Waves. *Ocean Engineering, Vol. 13, No. 1,* pp. 57-83.

Schäffer, H. A. (1993). Laboratory Wave Generation Correct to Second Order. *Wave Kinematics and Environmental Forces: Papers Presented at a Conference Organized by the Society for Underwater Technology and Held in London, U.K., 24–25 March 1993; Springer: Dordrecht, The Netherlands, 1993;* pp. 115–139.

Schäffer, H. A., Stolborg, T. and Hyllested, P. (1994). Simultaneous Generation and Active Absorption of Waves in Flumes, *International Symposium: Waves – Physical and Numerical Modelling, University of British Columbia, Vancouver, Canada.*

Schäffer, H. A. and Skourup, J. (1996). Active Absorption of Multidirectional Waves, *Proc., 25th Int. Conf. on Coastal Engineering, ASCE, New York.*

Schäffer, H. A. and Klopman, G. (2000). Review of Multidirectional Active Wave Absorption Methods.

Journal of Waterway, Port, Coastal and Ocean Engineering, Vol. 126, Issue 2, pp. 88-97.
Schäffer, H. A. and Steenberg, C. M. (2003). Second-order Wavemaker Theory for Multidirectional Waves, *Ocean Engineering, Vol. 30*, pp. 1203-1231.
Schäffer, H. A. and Jakobsen, K. P. (2003). Non-linear Wave Generation and Active Absorption in Wave Flumes, *Long waves symposium , Thessaloniki, Greece, 2003. (in parallel with XXX IAHR Congress).*
Tavakkol, S. and Lynett, P. (2017). Celeris: A GPU-accelerated open source software with a Boussinesq-type wave solver for real-time interactive simulation and visualization. *Computer Physics Communications, Vol. 217*, pp. 117.127.
Vincent, C. L. and Briggs, M. J. (1989). Refraction – Diffraction of Irregular Waves over a Mound. *Journal of Waterway, Port, Coastal and Ocean Engineering, Vol. 115, No. 2,* pp. 269-284.
Yang, Z., Liu, S., Bingham, H. B. and Li, J. (2014). Second-order coupling of numerical and physical wave tanks for 2D irregular waves. Part II: Experimental validation in two-dimensions. *Coastal Enginering, Vol 92,* pp. 61–74.
Yang, Z., Liu, S., Ji, X., Bingham, H. B. and Zhang, H. (2021). A generalized second-order 3D theory for coupling multidirectional wave propagation from a numerical model to a physical model. Part I: Derivation, implementation and model verification irregular waves. *Coastal Engineering, Vol 165*.
Zelt, J.A. and Skjelbreia, J. E. (1992). Estimating Incident and Reflected Wave Fields Using an Arbitrary Number of Wave Gauges. *Proceedings of the twenty-third int. conference on coastal engineering, New York*, pp. 777–789.
Zhang, H., Schäffer, H.A. and Jakobsen, K.P. (2007). Deterministic combination of numerical and physical coastal wave models. *Coastal Engineering, Vol 54,* pp. 171–186.